PERGAMON

Chaos, Solitons and Fractals 14 (2002) 269–291

CHAOS
SOLITONS & FRACTALS

www.elsevier.com/locate/chaos

Comparison of linear and nonlinear responses of a compliant tower to random wave forces

Seon Mi Han *, Haym Benaroya

Department of Mechanical and Aerospace Engineering, Rutgers, The State University of New Jersey, Piscataway, NJ 08855, USA

Accepted 1 October 2001

Abstract

A vertical member of a compliant offshore structure is modeled as a beam undergoing both bending and extension. The beam has a point mass and is subjected to a point axial load at the free end. The equations of motion for the axial and transverse displacements are nonlinear and coupled. A linear tension model is derived as a special case of the nonlinear coupled model with negligible axial displacement. The responses are obtained numerically for both models. A quarter of the International Ship and Offshore Structures Congress (ISSC) tension leg platform model is used as a numerical example. The free and forced responses obtained using the nonlinear coupled modeled are compared to those of the linear tension model.

1. Introduction

A compliant tower is an offshore structure used in the oil industry as an exploratory, production, oil storage, or oil landing facility. As opposed to fixed structures, compliant towers are flexible structures such that small displacements and deformations are allowed. Such structures are more difficult to model. However, the need for deeper ocean exploration and lower cost of construction has made compliant towers more popular in recent years. Examples of compliant towers that we consider are articulated towers and tension leg platforms (TLPs). Schematics are shown in Fig. 1.

One crucial characteristic of complaint towers is that they depend on high tension in the shaft or tendons for stability. Fixed structures, on the other hand, depend on structural rigidity for stability. High tension in complaint structures is provided by buoyancy chambers, pontoons, and hulls.

Reviews of the dynamic responses of compliant towers can be found in [1]. In modeling the vertical members of offshore towers, rigid body motion and bending are the primary components of the overall behavior. Therefore, most previous works have concentrated on either the rigid models, linear elastic models, or nonlinear transverse models. In the rigid model, the polar angle for 2D motions or two spherical angles for 3D motions can describe the motion completely. This model is often used with complex fluid forcing models in order to capture the nonlinear interactions between the fluid and structure. The rigid motions in 2D and 3D were studied by Jain and Kirk [2] and Bar-Avi and Benaroya [3,4]. In the linear and nonlinear transverse models, the transverse displacement as a function of axial location is sufficient to describe the motion. These models assume that the motion is small enough such that the coupling between the transverse and axial motions are negligible. Adrezin and Benaroya [5,6] examined the nonlinear transverse behavior with time dependent tension.

However, when the structure is long (more precisely when the slenderness ratio is large), the coupling between the axial and the transverse models may be large. The coupled axial and transverse vibrations of a compliant tower were

* Corresponding author.
E-mail addresses: shan@whoi.edu (S.M. Han), benaroya@rci.rutgers.edu (H. Benaroya).

0960-0779/02/$ - see front matter
PII: S0960-0779(01)00232-6

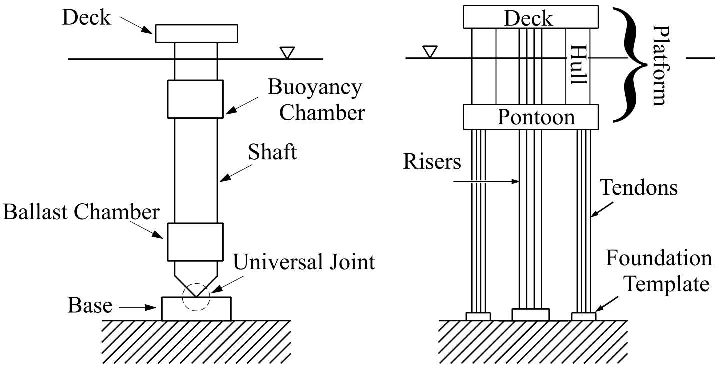

Fig. 1. Schematics of offshore structures.

previously studied by Yigit and Christoforou [7], and Han and Benaroya [8,9]. Yigit and Christoforou studied the coupled vibration of the oil well drillstrings in *compression*. The equations of motion were solved using the Assumed Mode Method. Han and Benaroya derived similar nonlinear coupled equations of motion and obtained the free and forced responses using the finite difference approach. In their studies, the point load N_o due to a buoyancy chamber at the free end was not included. This was because the numerical studies were performed based on a beam constructed by an experimental fluids group at Rutgers University led by Professor Timothy Wei.

In the current study, the point load at the free end is added to the nonlinear coupled axial and transverse equations of motion derived by Han and Benaroya since the tension provided by the buoyancy chamber is the most crucial element in the response of offshore structures. The purpose of this study is to compare the free and forced responses obtained by the linear transverse model and the nonlinear coupled model. For numerical purposes, a quarter of the International Ship and Offshore Structures Congress (ISSC) TLP is used. The slenderness ratio of this structure is 1904. The fluid force on the platform is due to random waves, and the random waves are modeled using the Pierson–Moskowitz spectrum and the Morison equation.

2. Mathematical formulation

2.1. Nonlinear coupled model

Fig. 2 shows a simplified model of an articulated tower or a quarter of a TLP. The shaft of an articulated tower or one leg of a TLP is modeled as a beam with length L, the deck as a point mass M_p, the buoyancy force provided by the buoyancy chamber and the gravity on the point mass as a point load N_o, and the joint at the ocean floor by a torsional

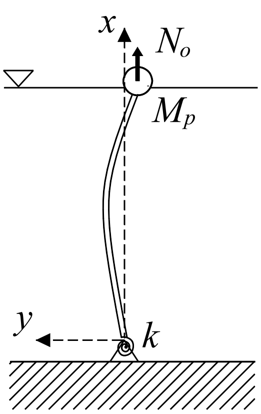

Fig. 2. A simplified model of a compliant tower.

spring with stiffness k. This model has the most essential physical features of a compliant tower. The motion is confined to a plane; motion in the third direction, out of the page in Fig. 2, is not allowed.

The governing equations of motion and boundary conditions are derived using Kirchhoff's hypothesis shown in Fig. 3 [8]. That is, in addition to the beam assumptions, we assume a displacement field given by

$$\begin{aligned} u_1(X,Y,t) &= u(X,t) - Y\frac{\partial v(X,t)}{\partial X}, \\ u_2(X,t) &= v(X,t), \\ u_3(X,t) &= 0, \end{aligned} \tag{1}$$

where X and Y are the Lagrangian coordinates, $u_{1,2,3}$ are the displacements in the x, y, and z directions, and u and v are the midplane displacements in the x and y directions. Note that they are functions of X and t only. Kirchhoff's hypothesis also implies that the strain is infinitesimal but rotation can be moderate. Mathematically, we can write

$$\frac{\partial u}{\partial X} \sim \left(\frac{\partial v(X,t)}{\partial X}\right)^2 \ll 0. \tag{2}$$

The kinetic energy of the corresponding displacement field is given by

$$\mathrm{KE} = \frac{1}{2}\int_0^L \left[\rho A\left(\dot{u}^2 + \dot{v}^2\right) + \rho I \dot{v}'^2\right] \mathrm{d}X + \frac{1}{2}M_{\mathrm{p}}\left(\dot{u}^2(L,t) + \dot{v}^2(L,t)\right), \tag{3}$$

where ρ is the density of the structure, A is the cross-sectional area of the beam, and I is the area moment of inertia about the neutral axis. Note that prime notation is used for the derivative with respect to X, and dot notation with respect to t.

The potential energy is given by

$$\mathrm{PE} = \int_0^L \left[\frac{EA}{2}\left(u' + \frac{1}{2}v'^2\right)^2 + \frac{EI}{2}v''^2\right] \mathrm{d}X + \frac{k}{2}v'^2(0,t), \tag{4}$$

where E is Young's modulus. The virtual work done is given by

$$\delta W = \int_0^L [p\delta u + f\delta v]\,\mathrm{d}X + N_{\mathrm{o}}\delta u(L,t), \tag{5}$$

where $p(X,t)$ and $f(X,t)$ are distributed loads in the x and y directions, respectively. The resulting governing equations of motion are given by [8,10]

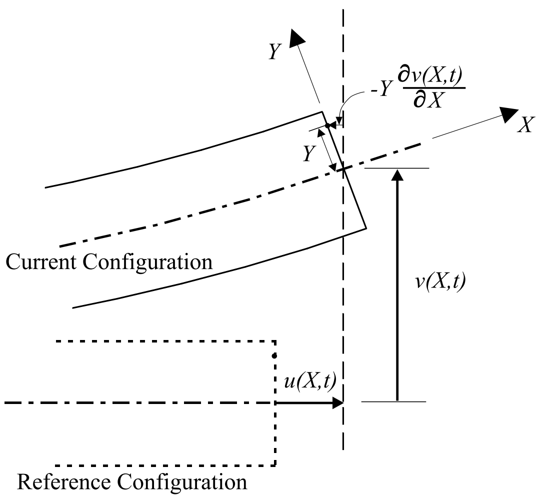

Fig. 3. Kirchhoff's hypothesis.

$$p(X,t) = \rho A\ddot{u} - \left(EA\left(u' + \frac{1}{2}v'^2\right)\right)', \tag{6}$$

$$f(X,t) = \rho A\ddot{v} - \left(EA\left(u' + \frac{1}{2}v'^2\right)v'\right)' - (\rho I\ddot{v}')' + (EIv'')'', \tag{7}$$

and the boundary conditions are given by

$$0 = u(0,t), \tag{8}$$

$$0 = \left[EA\left(u' + \frac{1}{2}v'^2\right) + M_p\ddot{u} - N_o\right]\Big|_{L,t}, \tag{9}$$

$$0 = v(0,t). \tag{10}$$

$$0 = EIv'' - kv'\big|_{0,t}, \tag{11}$$

$$0 = \left[\left(EIv''\right)' - \rho I\ddot{v}' - EA\left(u' + \frac{1}{2}v'^2\right)v' - M_p\ddot{v}\right]\Big|_{L,t}, \tag{12}$$

$$0 = EIv''(L,t). \tag{13}$$

If we include gravity and buoyancy in the equation, we can write

$$p(X,t) = \rho_f A_f g - \rho A g \tag{14}$$

and

$$N_o = \rho_f V_{\text{submerged}} g - M_p g, \tag{15}$$

where ρ_f is the density of the surrounding fluid, A_f is the cross-sectional area of the displaced volume of the beam,

$$A_f = \pi r_{\text{outer}}^2, \tag{16}$$

and $V_{\text{submerged}}$ is the submerged volume of the pontoon and the hull.

It should be noted that $u(X,t)$ and $v(X,t)$ are the displacements of a beam element from its original location X since the Lagrangian formulation is used. This is illustrated in Fig. 4.

The equations of motion are nonlinear and coupled. They need to be solved numerically. The responses are found using the finite difference approach.

2.2. Linear models

The derivation of the linear tension model using Newton's second law can be found in the text book by Meirovitch [11], and the derivation using a variational principle can be found in the text book by Benaroya [12]. Here, we will derive the equation of motion of the linear tension model by considering it as a special case of the nonlinear coupled model when the axial vibration can be neglected.

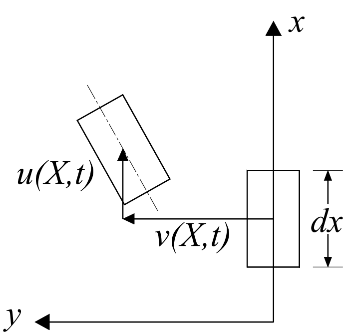

Fig. 4. Transverse and axial displacements.

Setting $u(X,t)=0$, the axial part of the equation of motion (Eq. (6)) is reduced to

$$\left(EA\frac{1}{2}v'^2\right)' = (\rho A - \rho_f A_f)g. \tag{17}$$

Integrating and using the boundary condition (9), we find that

$$EA\frac{1}{2}v'^2 = (\rho A - \rho_f A_f)g(X-L) + N_o. \tag{18}$$

The transverse part in Eq. (7) can be written as

$$\rho A\ddot{v} - \left[\{(\rho A - \rho_f A_f)g(X-L) + N_o\}v'\right]' - (\rho I(\ddot{v})')' + \left(EIv''\right)'' = f(X,t), \tag{19}$$

and the boundary conditions are reduced to

$$\begin{aligned}
0 &= v(0,t),\\
0 &= EIv'' - kv'\big|_{0,t},\\
0 &= \left(\left(EIv''\right)' - \rho I(\ddot{v})' - N_o v' - M_p\ddot{v}\right)\Big|_{L,t},\\
0 &= EIv''\big|_{L,t}.
\end{aligned} \tag{20}$$

The linearized equation of motion and the boundary conditions will be identical to the ones that can be found in Meirovitch and Benaroya if the gravitational and buoyance forces are omitted here.

If the transverse displacement is negligible in the overall response, $v=0$, we can recover the equation of motion and boundary conditions of the linear axial model given by

$$p(X,t) = \rho A\ddot{u} - \left(EAu'\right)' \tag{21}$$

and

$$\begin{aligned}
0 &= u(0,t),\\
0 &= \left[EAu' + M_p\ddot{u} - N_o\right]\Big|_{L,t}.
\end{aligned} \tag{22}$$

2.2.1. Analytical solution to the linear transverse model-free response

In this section, we will discuss a method to obtain the analytical solution to the linear transverse model when $p(X,t)$ and $f(X,t)$ are zeros. This section is meant to be an outline of the procedure. Detailed analysis for similar problems can be found in [12, Chapter 8].

We assume that the properties along the beam axis are uniform so that I, ρ, and E are constant. Then, the equation of motion in Eq. (19) is reduced to

$$\rho A\ddot{v} - N_o v'' - \rho I(\ddot{v})'' + EIv'''' = 0, \tag{23}$$

and the boundary conditions are given by

$$\begin{aligned}
0 &= v(0,t),\\
0 &= EIv'' - kv'\big|_{0,t},\\
0 &= \left(\left(EIv''\right)' - \rho I(\ddot{v})' - N_o v' - M_p\ddot{v}\right)\Big|_{L,t},\\
0 &= EIv''\big|_{L,t}.
\end{aligned} \tag{24}$$

First, assume that $v(X,t)$ is separable so that we can write $v(X,t) = V(X)F(t)$. Then, the equation of motion becomes

$$\rho AV\ddot{F} - N_o V''F - \rho IV''\ddot{F} + EIV''''F = 0. \tag{25}$$

Assuming that $F(t)$ is harmonic with frequency ω such that $\ddot{F}(t) = -\omega^2 F$ with solution $F(t) = a\sin\omega t + b\cos t$, we can write Eq. (25) as

$$EIV'''' + \left(\rho I\omega^2 - N_o\right)V'' - \rho A\omega^2 V = 0, \tag{26}$$

and the boundary conditions are written as

$$\begin{aligned} 0 &= V(0)F(t), \\ 0 &= \left(EIV'' - kV'\right)\big|_{X=0}F(t), \\ 0 &= \left(EIV''' + \rho I\omega^2 V' - N_{\mathrm{o}}V' + \omega^2 M_{\mathrm{p}}V\right)\big|_{X=L}F(t), \\ 0 &= EIV(L)''F(t). \end{aligned} \tag{27}$$

Since the boundary conditions must be satisfied at any time instance t, $F(t)$ can be factored out and $V(X)$ must satisfy the following boundary conditions:

$$\begin{aligned} 0 &= V(0), \\ 0 &= \left(EIV'' - kV'\right)\big|_{X=0}, \\ 0 &= \left(EIV''' + \rho I\omega^2 V' - N_{\mathrm{o}}V' + \omega^2 M_{\mathrm{p}}V\right)\big|_{X=L}, \\ 0 &= EIV(L)''. \end{aligned} \tag{28}$$

Assuming that $V(X)$ has the form

$$V(X) = c\mathrm{e}^{rX}, \tag{29}$$

we find that Eq. (26) becomes

$$EIr^4 + \left(\rho I\omega^2 - N_{\mathrm{o}}\right)r^2 - \rho A\omega^2 = 0. \tag{30}$$

The solutions to this fourth-order algebraic equation are

$$\begin{aligned} r_{1,2} &= \pm \mathrm{i}\sqrt{\frac{(\rho I\omega^2 - N_{\mathrm{o}}) + \sqrt{(\rho I\omega^2 - N_{\mathrm{o}})^2 + 4EI\rho A\omega^2}}{2EI}}, \\ r_{3,4} &= \pm\sqrt{\frac{-(\rho I\omega^2 - N_{\mathrm{o}}) + \sqrt{(\rho I\omega^2 - N_{\mathrm{o}})^2 + 4EI\rho A\omega^2}}{2EI}}, \end{aligned} \tag{31}$$

where the first two (r_1 and r_2) are imaginary and the last two (r_3 and r_4) are real. Then, the spatial solution becomes

$$V(X) = d_1 \sin\alpha X + d_2 \cos\alpha X + d_3 \sinh\beta X + d_4 \cosh\beta X, \tag{32}$$

where $d_1, \ldots, d_4$ are constants to be determined and

$$\begin{aligned} \alpha &= \sqrt{\frac{(\rho I\omega^2 - N_{\mathrm{o}}) + \sqrt{(\rho I\omega^2 - N_{\mathrm{o}})^2 + 4EI\rho A\omega^2}}{2EI}}, \\ \beta &= \sqrt{\frac{-(\rho I\omega^2 - N_{\mathrm{o}}) + \sqrt{(\rho I\omega^2 - N_{\mathrm{o}})^2 + 4EI\rho A\omega^2}}{2EI}}. \end{aligned} \tag{33}$$

Applying the boundary conditions in Eq. (28), we obtain four simultaneous equations which can be written in the matrix form as

$$[M]\{d\} = \{0\}. \tag{34}$$

In order to avoid the trivial solution, $d_1, \ldots, d_4$ must be linearly dependent or the determinant of $[M]$ must be zero. This equation, $\det([M]) = 0$, is also called the frequency equation and produces natural frequencies, $\omega_1, \omega_2, \omega_3, \ldots$ The constants d_2, d_3, and d_4 can be expressed in terms of d_1, and the value of d_1 is determined such that the eigenfunctions $V_n(X)$ are normalized with respect to ρA such that

$$\int_0^L \rho A W_n^2(X)\,\mathrm{d}X = 1. \tag{35}$$

Finally, the free response due to initial conditions is given by

$$v(X,t) = \sum_{n=1}^{\infty} V_n(X)(a_n \sin \omega_n t + b_n \cos \omega_n t), \tag{36}$$

where

$$\begin{aligned} b_n &= \int_0^L \rho A v(X,0) V_n(X)\,\mathrm{d}X, \\ a_n &= \frac{1}{\omega_n} \int_0^L \rho A \dot{v}(X,0) V_n(X)\,\mathrm{d}X. \end{aligned} \tag{37}$$

2.2.2. Analytical solution to the linear axial model-free response

In this section, the procedure to obtaining the free response of the linear axial model for a uniform beam. The equation of motion is given by (Eq. (21))

$$\rho A \ddot{u} - EAu'' = 0 \tag{38}$$

with boundary conditions

$$\begin{aligned} 0 &= u(0,t), \\ 0 &= [EAu' + M_\mathrm{p}\ddot{u} - N_\mathrm{o}]|_{L,t}. \end{aligned} \tag{39}$$

Note that the second boundary condition is not homogeneous. Letting $u(X,t) = w(X,t) + N_\mathrm{o}X/EA$, we have a equation of motion and homogeneous boundary conditions in terms of $w(X,t)$,

$$\rho A \ddot{w} - EAw'' = 0 \tag{40}$$

and

$$\begin{aligned} 0 &= w(0,t), \\ 0 &= [EAw' + M_\mathrm{p}\ddot{w}]|_{L,t}. \end{aligned} \tag{41}$$

First, we assume that $w(X,t)$ can be separated such that $w(X,t) = W(X)H(t)$ with harmonic $H(t)$. Then, the equation of motion and the boundary conditions for $W(X)$ becomes

$$EAW'' + \rho A \omega^2 W = 0 \tag{42}$$

and

$$\begin{aligned} 0 &= W(0), \\ 0 &= \left[EAW' - M_\mathrm{p}\omega^2 W\right]\big|_{L,t}. \end{aligned} \tag{43}$$

We find that the frequency equation is given by

$$\frac{EA}{M_\mathrm{p}}\sqrt{\frac{\rho}{E}} - \omega \tan \sqrt{\frac{\rho\omega^2}{E}}L = 0, \tag{44}$$

whose solutions are $\omega_1, \omega_2, \ldots$ The eigenfunction for corresponding natural frequency is given by

$$W_n(X) = d_n \sin \sqrt{\frac{\rho\omega_n^2}{E}}X. \tag{45}$$

The constant d_n are obtained by normalizing $W_n(X)$ with respect to ρA. Then, the solution is given by

$$w(X,t) = \sum_{n=1}^{\infty} W_n(X)(a_n \sin \omega_n t + b_n \cos \omega_n t), \tag{46}$$

where

$$\begin{aligned} b_n &= \int_0^L \rho A w(X,0) W_n(X)\,\mathrm{d}X, \\ a_n &= \frac{1}{\omega_n} \int_0^L \rho A \dot{w}(X,0) W_n(X)\,\mathrm{d}X \end{aligned} \tag{47}$$

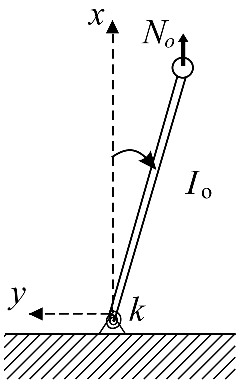

Fig. 5. Rigid model.

and

$$w(X,0) = u(X,0) - N_o X/EA,$$
$$\dot{w}(X,0) = \dot{u}(X,0). \tag{48}$$

The final solution $u(X,t)$ is given by

$$u(X,t) = \sum_{n=1}^{\infty} W_n(X)\left[\left(\frac{1}{\omega_n}\int_0^L \rho A\dot{u}(X,0)W_n(X)\,\mathrm{d}X\right)\sin\omega_n t + \left(\int_0^L \rho A(u(X,0) - N_o X/EA)W_n(X)\,\mathrm{d}X\right)\cos\omega_n t\right] + N_o X/EA. \tag{49}$$

2.2.3. Rigid model

It should be noted that the system responds as a soft spring system. This can be shown by looking at the rigid model in Fig. 5. The equation of motion for this system is given by

$$I\ddot{\theta} + k\theta + N_o L\sin\theta = 0. \tag{50}$$

$\sin\theta$ can be expanded about $\theta = 0$ so that the equation of motion can be approximated as

$$I\ddot{\theta} + (k + N_o L)\theta - N_o L\frac{\theta^3}{3!} = 0. \tag{51}$$

Since the sign of the cubic term is negative, the system behaves as a soft spring system. That is, the restoring force of this nonlinear system, $(k + N_o L)\theta - N_o L\theta^3/3!$, is less than the restoring force of an equivalent linear system, $(k + N_o L)\theta$.

3. Formulation of transverse load due to random waves

In this section, the transverse forcing function, $f(X,t)$, is formulated to represent practical loading situations. Let us assume that a beam is submerged in water and is subjected to current and waves. The beam is constrained to vibrate in the direction of the flow, allowing motion in one plane only.

The transverse force is formulated using Morison's equation and is given by [13]

$$f(X,t) = -C_A\rho_f\pi r_o^2\ddot{R}_n + C_M\rho_f\pi r_o^2\dot{w}_n + C_D\rho_f r_o(w_n + U_n - \dot{R}_n)|w_n + U_n - \dot{R}_n|, \tag{52}$$

where $\dot{R}$ is the velocity of the beam, w is the wave velocity, and U is the current velocity. The subscript n is used to indicate that they are the normal component (normal to the structure). C_A is the added mass coefficient, C_D is the drag coefficient, and C_M is the inertia coefficient. r_o is the outer radius of the structure. Note that Morison's equation is applicable when the drag force is predominant, which is the case when the structural diameter is small compared to the water wave length [14].

The first term in Eq. (52) is the added mass term, the second is the inertial term, and the third is the drag term. The added mass effect results from some of the fluid particles being permanently displaced by the motion of the cylinder. The inertia force is the force exerted by the fluid when the fluid accelerates and decelerates as it passes around a circular cylinder, or it is the force required to hold a cylinder stationary in a flow of uniform acceleration. The drag force is due to the pressure difference between the downstream and upstream regions.

The normal component of the structure, wave and current velocities can be obtained by dotting the velocity vectors with the normal vector (normal to the structure) such that we can write

$$\begin{aligned} \dot{R}_n &= -\dot{u}v' + \dot{v}, \\ \dot{R}_n &= -\ddot{u}v' + \ddot{v}, \\ w_n &= -w_x v' + w_y, \\ U_n &= -U_x v' + U_y. \end{aligned} \tag{53}$$

The next step is to find the expressions for the wave and current velocities.

We assume that the current flows in the horizontal (y) direction with constant velocity. In order to obtain the wave velocities and accelerations, we use the Airy linear wave theory and the Pierson–Moskowitz spectrum. From the Airy linear wave theory, for the wave elevation given by

$$\eta(y,t) = A\cos(ky - \omega t), \tag{54}$$

the corresponding wave velocities are given by

$$\begin{aligned} w_y(x,y,t) &= A\omega \frac{\cosh kx}{\sinh kd}\cos(ky - \omega t), \\ w_x(x,y,t) &= A\omega \frac{\sinh kx}{\sinh kd}\sin(ky - \omega t) \end{aligned} \tag{55}$$

with the dispersion relation given by

$$\omega^2 = gk\tanh kd. \tag{56}$$

Note that the Airy wave theory assumes that the wave height is small compared to the wave length or water depth [15].

The wave elevation η, in reality, has more than one frequency components, and these frequencies may have different 'strengths'. The frequency content is expressed in terms of a power spectrum. There are many models for the spectrum for the wave height in an ocean environment. A summary of existing models can be found in [15]. Here, we use the one-sided Pierson–Moskowitz spectrum whose expression is given by

$$S(\omega) = \frac{0.0081g^2}{\omega^5}\exp\left[-0.74\left(\frac{g}{U_{\mathrm{w}}\omega}\right)^4\right] \ (\mathrm{m}^2\ \mathrm{s}). \tag{57}$$

The Pierson–Moskowitz spectrum depends on one physical parameter, the wind speed U_{w}. For our purpose, it is easier to use a parameter called the significant wave height H_{s}. The significant wave height is the average of the height of the highest one-third of all waves [16]. Mathematically, it is four times the variance (Eq. 4.62 in [15]). The significant wave height is related to the wind speed by

$$H_{\mathrm{s}} = \frac{0.20924U_{\mathrm{w}}^2}{g}. \tag{58}$$

The Pierson–Moskowitz spectrum, in terms of H_{s}, is given by

$$S(\omega) = \frac{0.7795}{\omega^5}\mathrm{e}^{-(3.12/H_{\mathrm{s}}^2)\omega^{-4}} \ (\mathrm{m}^2\mathrm{s}). \tag{59}$$

The frequency at which the power spectrum is maximum is given by

$$\omega_{\mathrm{peak}} = \frac{1.2568}{\sqrt{H_{\mathrm{s}}}} \ (\mathrm{rad/s}). \tag{60}$$

Fig. 6 shows the Pierson–Moskowitz spectrum for $H_{\mathrm{s}} = 12$, 15, 19 m, and Table 1 shows the corresponding wind velocities and the peak frequencies.

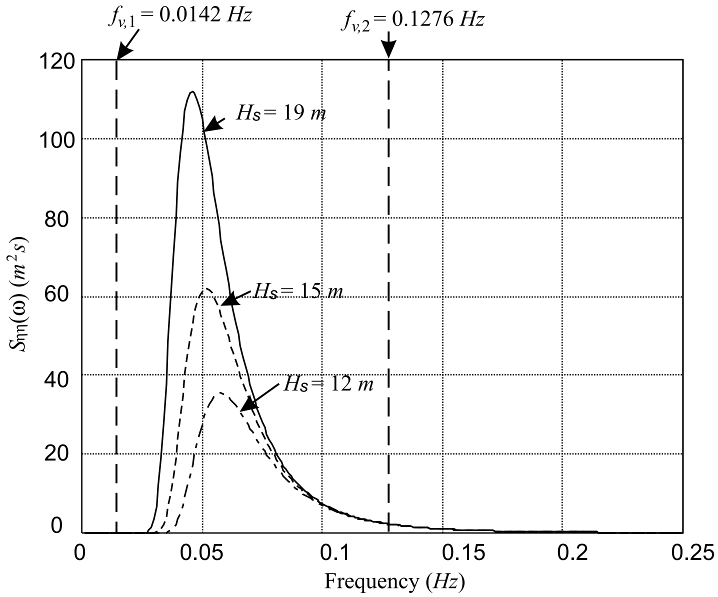

Fig. 6. The Pierson–Moskowitz spectrum, $H_s = 12$, 15, 19 m.

Table 1
Significant wave heights, wind speeds, and peak frequencies

H_s (m)	U_w (m/s, mph)	ω_{peak} (rad/s, Hz)
12	23.7, 53.1	0.363, 0.0578
15	26.5, 59.3	0.325, 0.0517
19	29.8, 66.8	0.288, 0.0458

The wave height in time domain is given by [12]

$$\eta(y,t) = \int_0^\infty \cos(ky - \omega t)\sqrt{2S(\omega)\,\mathrm{d}\omega}. \tag{61}$$

In order to carry out the integration, we used the method suggested by Borgman [17]. The integral is represented as a finite sum by dividing the power spectrum in N equal areas. After mathematical manipulations, the wave height is given by

$$\eta(y,t) = \frac{H_s}{4}\sqrt{\frac{2}{N}}\sum_{n=1}^{N} \cos\left(\bar{k}_n y - \bar{\omega}_n t\right), \tag{62}$$

where N is the number of intervals and $\bar{\omega}_n$ is the average value of angular frequency at nth interval. $\bar{k}_n$ is the wave number that corresponds to $\bar{\omega}_n$. It is obtained using the dispersion relationship in Eq. (56). Using the Airy wave theory, the wave velocities are given by

$$\begin{aligned} w_y(x,y,t) &= \frac{H_s}{4}\sqrt{\frac{2}{N}}\sum_{n=1}^{N} \bar{\omega}_n \frac{\cosh \bar{k}_n x}{\sinh \bar{k}_n d} \cos\left(\bar{k}_n y - \bar{\omega}_n t\right), \\ w_x(x,y,t) &= \frac{H_s}{4}\sqrt{\frac{2}{N}}\sum_{n=1}^{N} \bar{\omega}_n \frac{\sinh \bar{k}_n x}{\sinh \bar{k}_n d} \sin\left(\bar{k}_n y - \bar{\omega}_n t\right). \end{aligned} \tag{63}$$

The only variable to be specified to determine the wave velocities is the significant wave height. The wave accelerations are obtained by taking time derivatives.

4. Results and discussion

For numerical purposes, we first consider a beam whose numerical values are based on a quarter of the TLP model from the ISSC Derived Loads Committee I.2 developed in 1985 [1,18]. The properties of the ISSC model are given in Table 2. The free responses due to nonzero initial conditions are obtained using the nonlinear coupled model and the linear model. The linear model is solved analytically using the method of separation of variables and eigenfunction expansion. The nonlinear coupled model is solved numerically using the finite difference approach. The finite difference equations are written for the spatial derivatives for N nodes to yield the equations of motion in terms of $2N$ second-order differential equations in time. MATLAB function ode45.m is used to solve the resulting ordinary differential equations. The function ode45.m solves ordinary differential equations with initial conditions using fourth- or fifth-order Runge–Kutta method. 14 nodes are used here.

The physical properties of the TLP yield the combined terms shown in Table 3.

Buoyancy is provided by the pontoon and hull. Assuming that the pontoon is completely submerged under water and the hull is partially submerged, the displaced volume is given by

$$V_{\mathrm{submerged}} = P_{\mathrm{h}}P_{\mathrm{d}}P_{\mathrm{l}} + \frac{\pi}{4}H_{\mathrm{d}}^2(D_{\mathrm{w}} - L - u(L,t)) = 13\,300 - 223.8u(L,t), \tag{64}$$

where $D_{\mathrm{w}} - L - u(L,t)$ represents the submerged length of the hull. From Eq. (15), we find that

$$N_{\mathrm{o}} = 3.462\mathrm{e}7 - 2.250\mathrm{e}6 \times u(L,t). \tag{65}$$

For the linear tension model, we can let $u(L,t) = 0$ such that N_{o} for the linear tension model is 3.462e7 N.

4.1. Free response

Let us first consider the response when $f(X,t) = p(X,t) = 0$. The equation of motion for the linear transverse model is given by

Table 2
Properties of the TLP (quarter ISSC based model) and the surrounding fluid

Property	ISSC model
Tendon length, L	415.0 m
Tendon outer radius, r_{o}	0.4000 m
Tendon inner radius, r_{i}	0.1732 m
Tendon density, ρ	7800 kg/m^3
Young's modulus of a tendon, E	204.0 GPA
Hull mass, M_{p}	10.10e6 kg
Hull diameter, H_{d}	16.88 m
Hull length, H_{l}	67.50 m
Pontoon height, P_{h}	10.50 m
Pontoon depth, P_{d}	7.500 m
Pontoon length, P_{l}	69.37 m
Water depth, D_{w}	450.0 m
Density of water, ρ_{f}	1025 kg/m^3

Table 3
Properties of the simplified model

	ISSC model
ρA	3.186e3 kg/m
EI	3.957e9 N m^2
EA	8.168e10 kg/m s^2
ρI	151.3 kg m
M_{p}	1.010e7 kg
$\rho_{\mathrm{f}}A_{\mathrm{f}}$	515.22 kg/m
N_{o}	3.462e7 N

$$\rho A\ddot{v} - N_o v'' - \rho I\ddot{v}'' + EIv'''' = 0 \tag{66}$$

with boundary conditions given by

$$\begin{aligned} 0 &= v(0,t), \\ 0 &= EIv'' - Kv'|_{0,t}, \\ 0 &= (EIv''' - \rho I\ddot{v}' - N_o v' - M_p\ddot{v})|_{L,t}, \\ 0 &= EIv''|_{L,t}. \end{aligned} \tag{67}$$

The linear axial equation of motion is given by

$$\rho A\ddot{u} - EAu'' = 0, \tag{68}$$

and the corresponding boundary conditions are given by

$$\begin{aligned} 0 &= u(0,t), \\ 0 &= [EAu' + M_p\ddot{u} - N_o]|_{L,t}. \end{aligned} \tag{69}$$

These linear equations of motion can be solved analytically, and the natural frequencies are given by

$$\begin{aligned} f_v &= 0.0142, 0.1276, 0.2552, 0.3880, 0.5279, 0.6768, \\ &\quad 0.8363, 1.1936, 1.3937, 1.6094, 1.8415, 2.0906, 2.3573, \ldots \ \text{(Hz)}, \\ f_u &= 0.6876, 6.1807, 12.2420, 18.3294, 24.4236, \\ &\quad 30.5204, 36.6185, 42.7174, 48.8168, \ldots \ \text{(Hz)}. \end{aligned} \tag{70}$$

The first two natural frequencies of the linear transverse model are shown in Fig. 6 with input frequency spectrum.

Now, let us consider the responses predicted by the nonlinear model. The equations of motion and the boundary conditions are given in Eqs. (6)–(13) with $f(X,t)$ and $p(X,t)$ set to zero. The initial velocities are set to zero and the initial displacements are given by

$$\begin{aligned} v(X,0) &= 0.0004X^2/L, \\ u(X,0) &= -0.0004234X. \end{aligned} \tag{71}$$

The displacements correspond to the initial configuration when the beam is subjected to an end moment shown in Fig. 7. This particular set of initial conditions are known to produce a response with frequencies other than the first few natural frequencies [8,9]. Note that this set satisfies the equation of motion and the boundary conditions of the nonlinear coupled model, namely Eqs. (6) and (9).

In this particular case, the transverse and the axial displacements at $X = L$ are comparable in magnitude. Theoretically, the linear tension model may have trouble predicting the response or the natural frequency for this case since the linear tension model is valid when the axial motion is negligible compared to the transverse model. We are interested

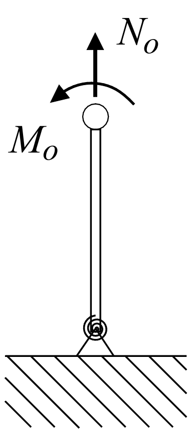

Fig. 7. Initial configuration.

in how well the linear model can predict the natural frequencies even in this extreme condition. Fig. 8 shows the transverse displacements at $X = L$ predicted by the nonlinear coupled model.

From the displacement plot, the fundamental frequency of the transverse model is 1/70.66 s or 0.01415 Hz. The power spectral density plot of the transverse displacement in Fig. 9 also shows a peak at around 0.0140 Hz. The power spectral density also shows the natural frequencies other than the ones obtained by the linear model in Eq. (70). Since 14 nodes are used for v and u, we expect to see up to 28 frequencies. Fig. 10 shows the same power spectral density plot up to 1 Hz. The frequencies are

$$\begin{aligned} f_v = {} & \mathbf{0.0140}, \mathbf{0.1275}, \mathbf{0.2533}, 0.3064, \mathbf{0.3815}, 0.5082, 0.5600, \\ & 0.6373, 0.6728, 0.7018, 0.7643, 0.8150, 0.8869, \ldots \quad (\mathrm{Hz}). \end{aligned} \tag{72}$$

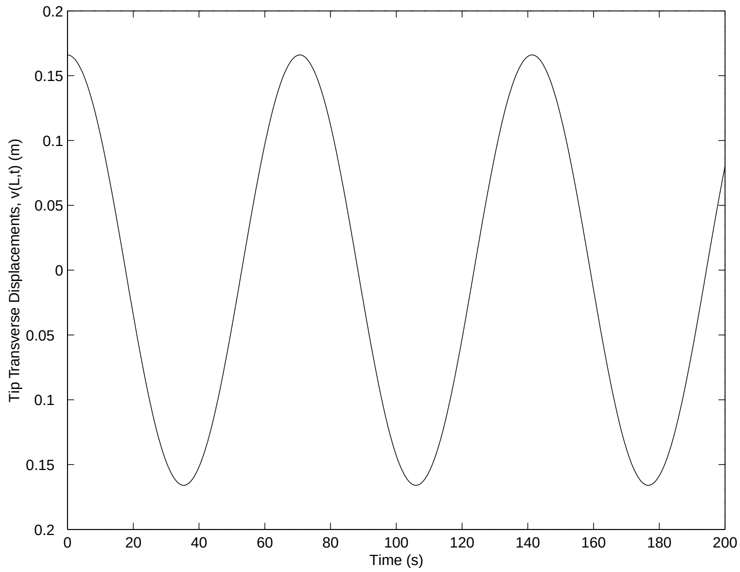

Fig. 8. Free response: transverse displacement $v(L, t)$ predicted by the nonlinear coupled model.

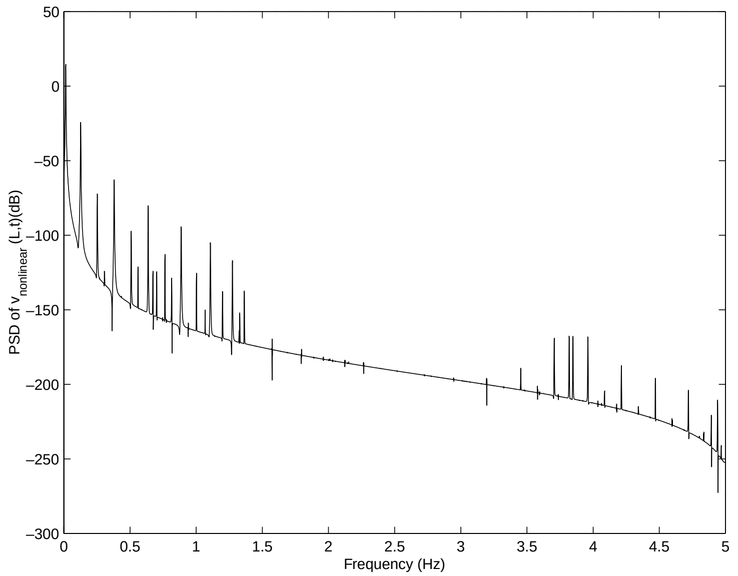

Fig. 9. Free response: power spectral density plot of $v(L, t)$ predicted by the nonlinear coupled model.

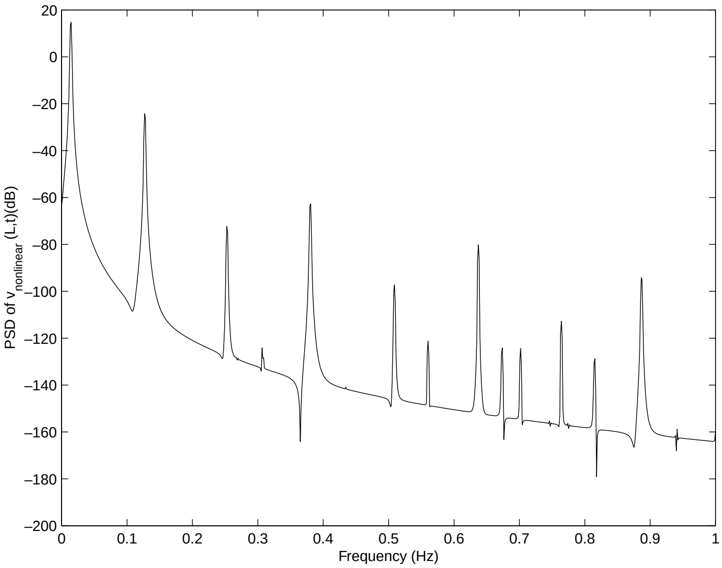

Fig. 10. Free response: power spectral density plot of $v(L,t)$ predicted by the nonlinear coupled model for $0 < f < 1$ Hz.

The power spectral density plot is obtained using 8192 data points sampled at 10 Hz, which results in the resolution of 0.0012207 Hz. Therefore, the reading error is about ± 0.0006 Hz, which is half the resolution. Comparing the natural frequencies with the ones obtained using the linear model in Eq. (70), we can find corresponding frequencies at the lower frequency levels. The frequencies in bold print in Eq. (72) are the frequencies that are also obtained in the linear tension model. For example, the third natural frequency, 0.2533 Hz, corresponds to the third natural frequency of 0.2552 Hz in the linear model. Due to this reading error, it is hard to say whether the motion predicted by the nonlinear model is faster or slower than the motion predicted by the linear model. As the frequency increases, the two models show more deviation. In addition, certain natural frequencies are not captured by the linear model. However, it is remarkable that the linear tension model can predict the first three natural frequencies very accurately even when the axial motion is not negligible.

Fig. 11 shows the axial displacement at $X = L$ predicted by the nonlinear coupled model. The axial displacement plot shows the two dominant frequencies at 0.028 and 0.688 Hz. The first frequency is twice the first natural frequency of the transverse motion, and the second is close to the natural frequency of the linear axial model in Eq. (70). The reason why the axial displacement has twice the fundamental frequency of the transverse motion was explained by Han and Benaroya [8,9]. The reason becomes clear when we look at Fig. 13. When the beam vibrates around the vertical axis tracing points $1 \to 2 \to 3 \to 2 \to 1$, the transverse displacement makes one cycle while the axial displacement makes two.

The power spectral density plot for $u(L,t)$ in Fig. 12 shows the frequencies at

$$f_u = 0.02805, 0.1123, 0.1148, 0.2551, 0.3650, 0.3674, 0.3800, \\ 0.5078, 0.6225, 0.6330, 0.6512, \mathbf{0.6879}, 0.7611, \ldots \quad \text{(Hz)}. \tag{73}$$

Again, the reading error is about ± 0.0006 Hz. The linear model can predict only one frequency in this frequency range, namely 0.6879 Hz. Note that some of these frequencies also show up in the transverse motion.

Now, let us examine the strain in each case. The expression for the normal strain is given by [1]

$$\begin{aligned} \mathscr{E}_{XX} &= u' + \frac{1}{2}v'^2 - Yv'' \quad \text{for the nonlinear coupled model,} \\ \mathscr{E}_{XX} &= \frac{N_o}{EA} - Yv'' \quad \text{for the linear tension model,} \end{aligned} \tag{74}$$

[1] The expression for Green's strain for the nonlinear coupled model is obtained from the Kirchhoff's displacement field. Refer to [8].

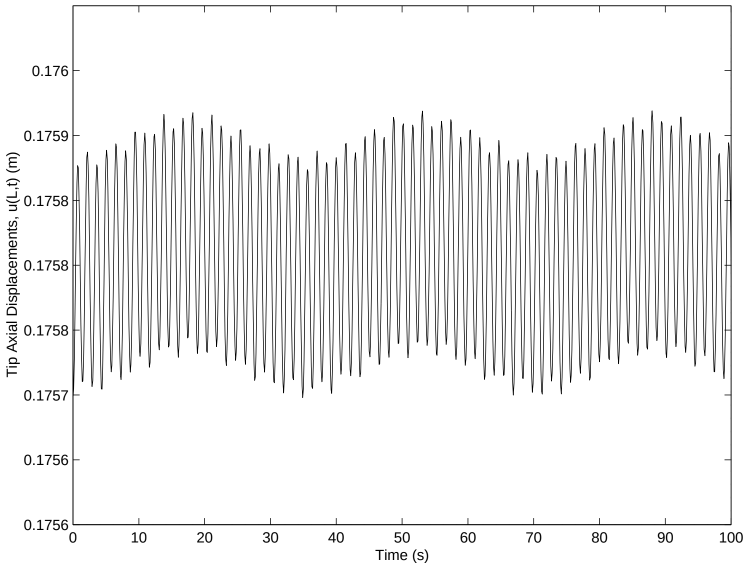

Fig. 11. Free response: axial displacement $u(L,t)$ predicted by the nonlinear coupled model.

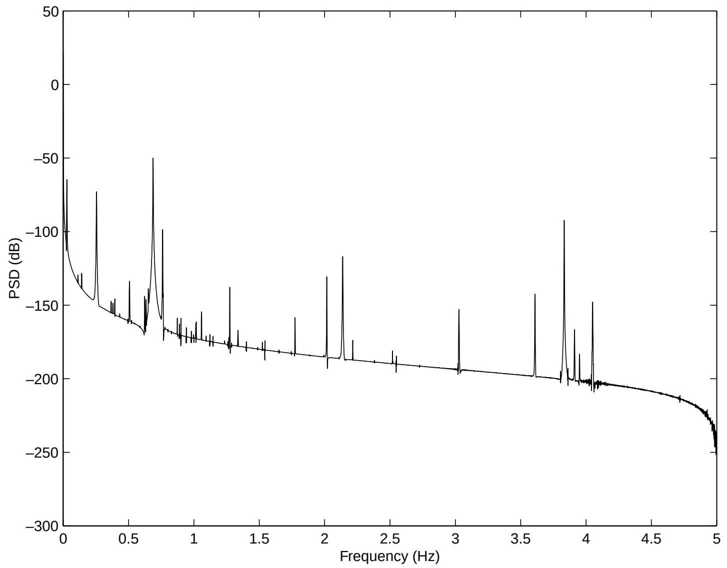

Fig. 12. Free response: power spectral density plot of $u(L,t)$ predicted by the nonlinear coupled model.

where Y is the distance from the neutral axis or the midplane. The stress is then obtained by multiplying the strain by Young's modulus. At the midplane, $Y = 0$, the stress predicted by the linear tension model is constant and is equal to

$$\sigma_{XX}(X, Y = 0) = \frac{N_o}{A}. \tag{75}$$

Fig. 14 shows the normal midplane stress at $X = L$. The stress predicted by the linear tension model is approximately the average stress predicted by the nonlinear model.

The free vibration analysis shows that the linear tension model is capable of predicting the transverse displacement and the average stress very well even when the axial displacement is not negligible compared to the transverse displacement.

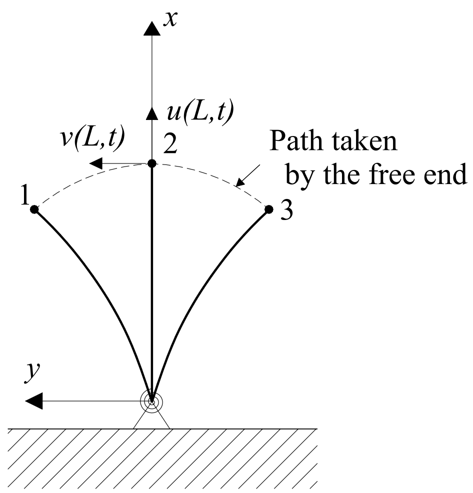

Fig. 13. Typical paths taken by the free end.

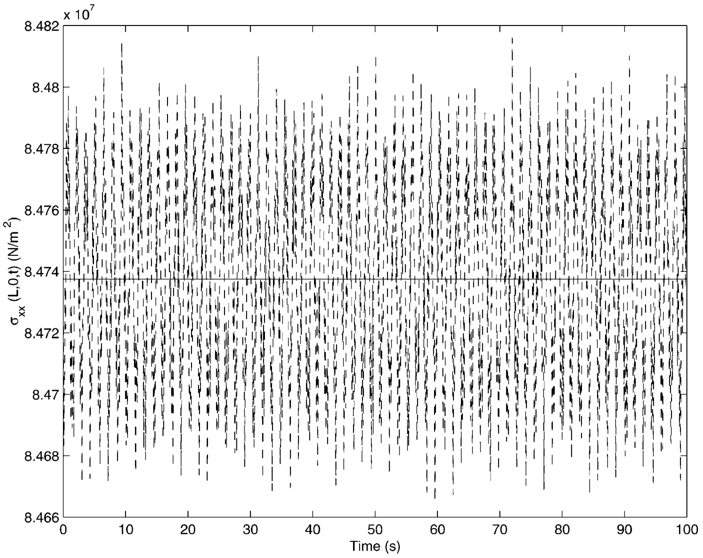

Fig. 14. Free response: midplane stress at $X = L$, $\sigma_{XX}(L, 0, t)$.

4.2. Forced response due to gravity and random waves

Let us consider responses in the presence of gravity and random waves. The distributed loads, $p(X, t)$ and $f(X, t)$, are given in Eqs. (14) and (52). Here, we will consider two cases: $H_s = 19$ m with zero and nonzero initial conditions. Let us keep in mind that the peak frequency is at 0.0458 Hz, and the fundamental frequency from the free vibration is at 0.01415 Hz.

4.2.1. Case I. Zero initial conditions

Fig. 15 shows the transverse displacements when zero initial conditions are used. The transverse displacements predicted by the linear tension and nonlinear coupled models start out similar but diverge after a while. Fig. 16 shows the power spectral density plots for the transverse displacements. Again, the power spectral density plot is obtained using 8192 data points sampled at 10 Hz. Comparing them with the power spectral plot of the free response in Figs. 9 and 10, we notice that the power in the forced response is distributed in a broad spectrum. This is due to the fact that

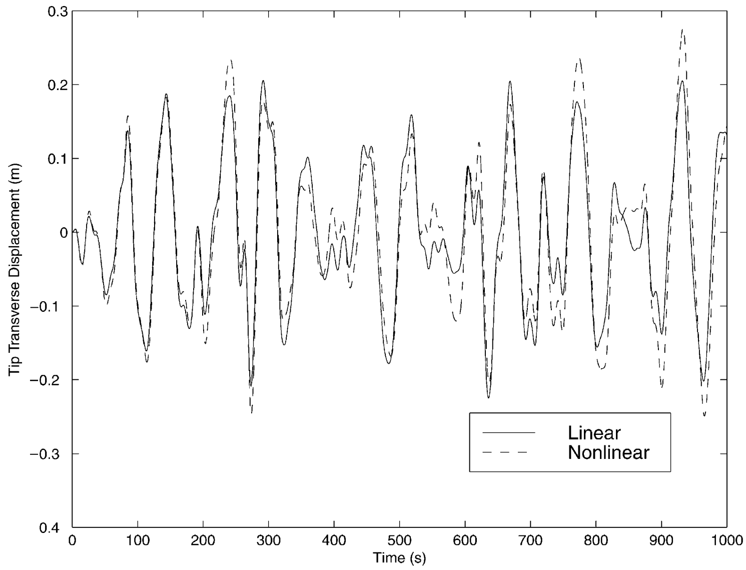

Fig. 15. Forced response: $v(L,t)$ when $H_s = 19$ m and $v(X,0) = \dot{v}(X,0) = 0$.

the forcing frequencies themselves are broad as shown in Fig. 6. The power spectra for the linear and the nonlinear responses are similar for the most part except at frequencies around 0.7, 1.3, 2.1, 3.2 and 3.8 Hz. These frequencies also appeared in the free response predicted by the nonlinear model in Fig. 12. Therefore, these frequencies are natural frequencies that the linear model is not able to locate.

Fig. 17 shows the same power spectral density plot for frequencies between 0 and 0.5 Hz. For this range of frequency, the power spectral densities of the linear and nonlinear models are quite similar. They both show the fundamental frequency at around 0.02 Hz, and the forcing frequencies of the random waves peaking between 0.04 and 0.05 Hz. [2] The two lowest peaks appear close to each other suggesting that we may have a beating. Looking at the transverse displacement plots in Fig. 15 again, we do see irregular beating.

Figs. 18 and 19 show the axial displacement and its power spectral density plot predicted by the nonlinear coupled model. The figures show a distinctive peak at 0.6880 Hz. The frequencies lower than that are harder to distinguish due to the spectrum of forcing frequencies around $f_{\text{peak}} = 0.0458$ Hz.

It should be noted that both transverse and axial motion do not seem to be influenced by the fluid damping force.

4.2.2. Case 2. Nonzero initial conditions

Let us consider initial conditions given by

$$\begin{aligned} v(X,0) &= 0.05X, \\ u(X,0) &= -0.0008263X, \end{aligned} \tag{76}$$

with zero initial velocities. Fig. 20 shows the transverse displacements, and Figs. 21 and 22 show the power spectral density plots for $v(L,t)$. We notice that the irregular beating phenomenon can no longer be observed in these plots. Instead, we see a damped motion oscillating primarily at one frequency. The transverse motion predicted by the nonlinear model, $v_{\text{nonlinear}}(L,t)$, primarily oscillate at 0.0128 Hz, and $v_{\text{linear}}(L,t)$ oscillates at 0.0131 Hz which is slightly faster than $v_{\text{nonlinear}}(L,t)$. Both frequencies are lower than the fundamental frequency. When the initial displacements are set to nonzero values, the damping force increases therefore decreasing the frequency of oscillation.

It should be noted that we expect that v_{linear} oscillates faster than $v_{\text{nonlinear}}$. The nonlinear coupled model is more 'flexible' than the linear tension model because it allows the beam to deform in the axial direction in addition to the transverse direction. Therefore, the response predicted by the nonlinear coupled model should be slower than that predicted by the linear tension model.

[2] The actual peak frequency is 0.0458 Hz.

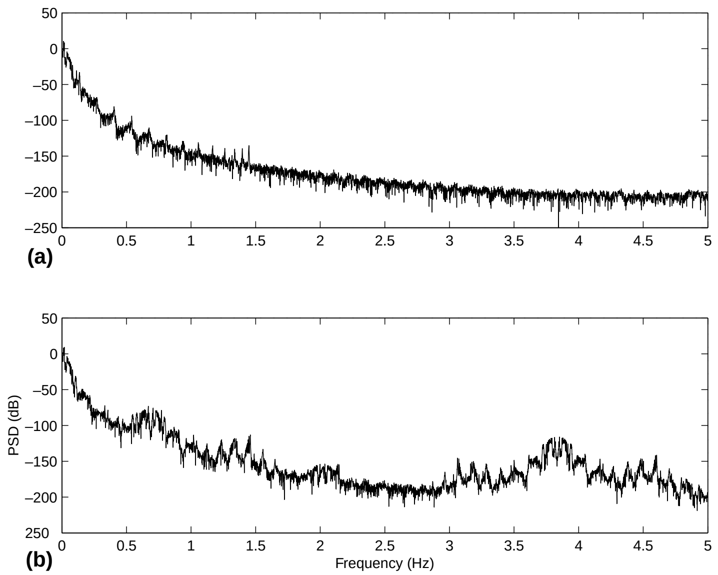

Fig. 16. Forced response: power spectral density plots for $v(L,t)$ predicted by the linear tension and nonlinear coupled models when $H_s = 19$ m and $v(X,0) = \dot{v}(X,0) = 0$. (a) PSD plot for $v_{\text{linear}}(L,t)$, (b) PSD plot for $v_{\text{nonlinear}}(L,t)$.

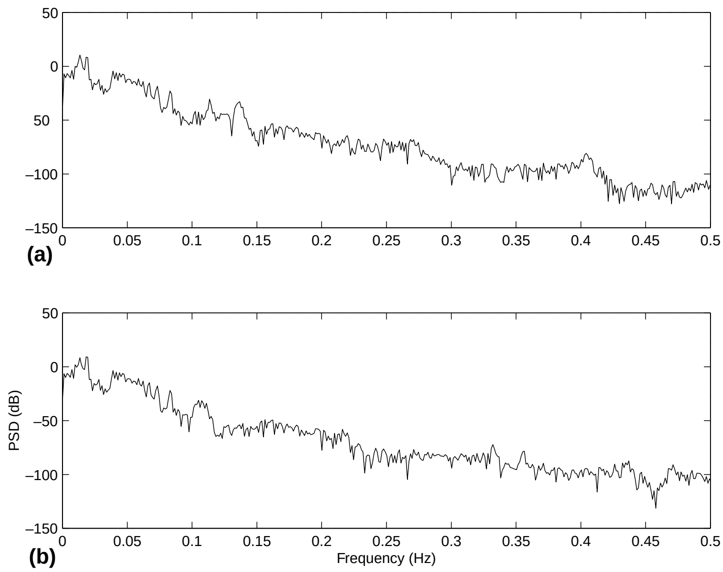

Fig. 17. Forced response: power spectral density plots for $v(L,t)$ predicted by the linear tension and nonlinear coupled models when $H_s = 19$ m and $v(X,0) = \dot{v}(X,0) = 0$ for $0 < f < 0.5$ Hz. (a) PSD plot for $v_{\text{linear}}(L,t)$, (b) PSD plot for $v_{\text{nonlinear}}(L,t)$.

Also, the forcing frequencies do not show in the displacement plot, and most of the power is at the fundamental frequency. What we observe here is subharmonic resonance of order 1/2, where the system responds at the natural frequency when the forcing frequency is near twice the natural frequency. Subharmonic resonance only appears for a particular range of forcing frequencies and initial conditions. That is, if the forcing frequencies are higher or lower than what we have now, we may not observe the subharmonic resonance at all. Instead, we may see both the damped natural frequencies and the forcing frequencies in the response plot.

Figs. 23 and 24 show the axial displacement and its power spectral density. The motion is damped and oscillates primarily at 0.0257 and 0.6880 Hz, the first being twice the first damped natural frequency of the transverse motion and

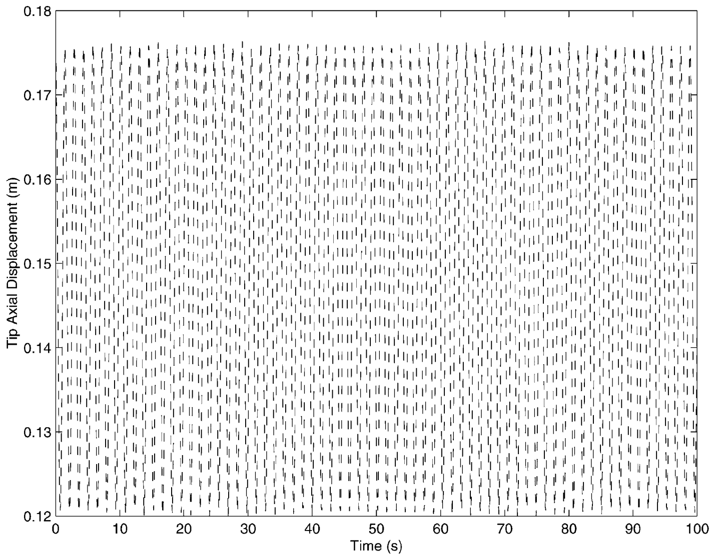

Fig. 18. Forced response: $u(L,t)$ predicted by the nonlinear coupled model when $H_s = 19$ m and $v(X,0) = \dot{v}(X,0) = 0$.

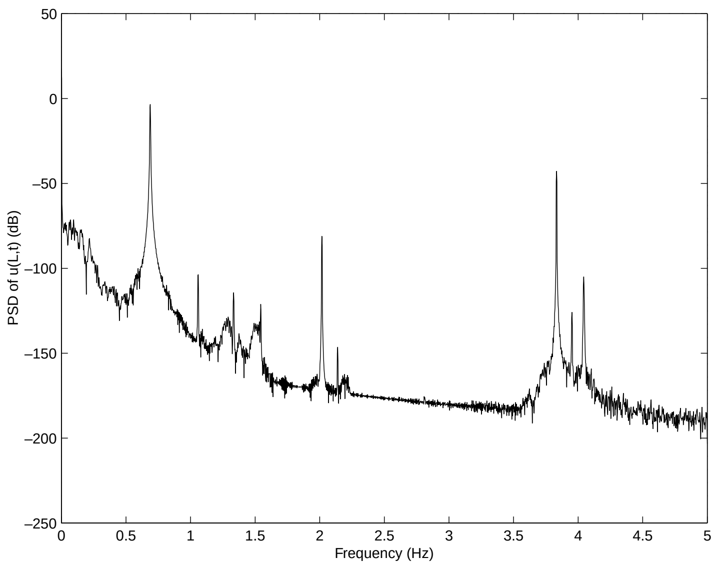

Fig. 19. Forced response: power spectral density plot of $u(L,t)$ when $H_s = 19$ m and $v(X,0) = \dot{v}(X,t) = 0$.

the second the fundamental frequency of the axial motion. Note that the axial motion damps only to a certain degree. It was shown by Han and Benaroya [8,9] that as the transverse motion damps out, the effect of the Morison fluid force on the axial motion also diminishes. Therefore, even after the transverse motion damps out completely, the axial motion will persist.

5. Summary and conclusion

1. In the free response, the initial displacements are chosen such that the transverse and axial displacements are of the same order. It is observed that the both models produce similar power spectral density plots for the transverse

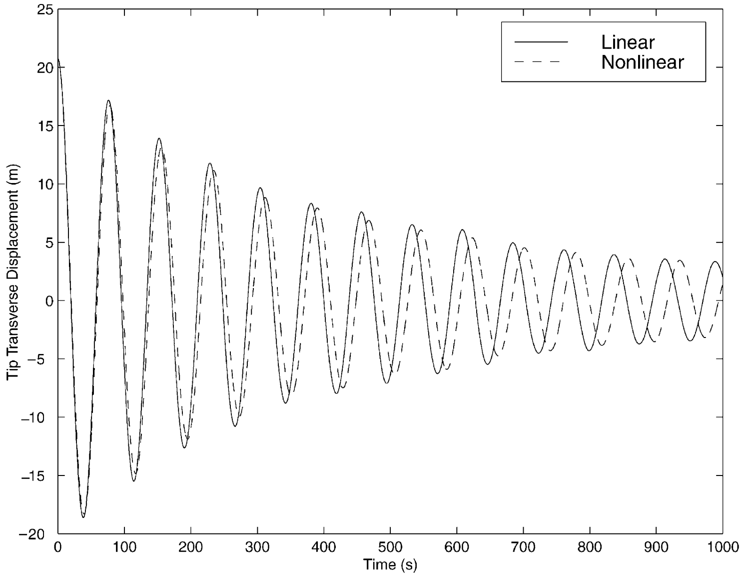

Fig. 20. Forced response: $v(L,t)$ when $H_s = 19$ m, $v(X,0) = 0.05X$ and $\dot{v}(X,t) = 0$.

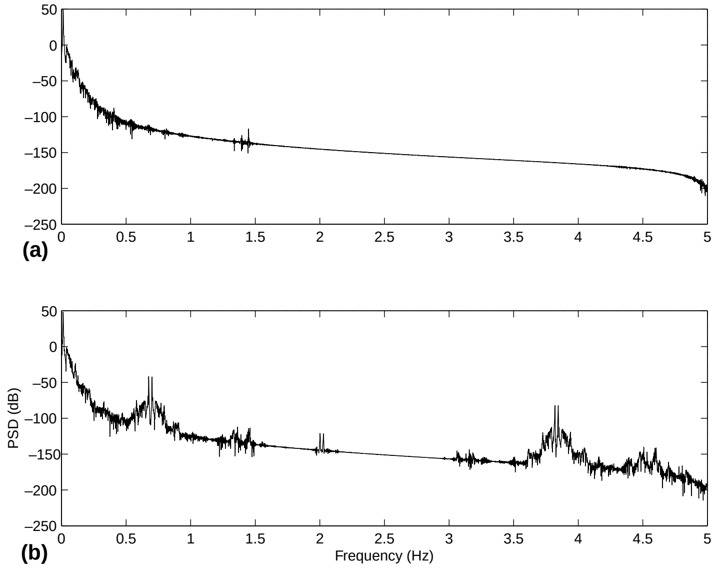

Fig. 21. Forced response: power spectral density plot of $v(L,t)$ when $H_s = 19$ m, $v(X,0) = 0.05X$ and $\dot{v}(X,t) = 0$. (a) PSD plot for $v_{\text{linear}}(L,t)$, (b) PSD plot for $v_{\text{nonlinear}}(L,t)$.

displacement at low frequencies for this particular case. As a result, the transverse displacements predicted by both models look identical. Therefore, for most cases where the energy is concentrated at the lower frequencies and cases where we are only interested in the transverse response, the linear tension model is as good as the nonlinear coupled model. This result was unexpected because the linear tension model is valid only when the axial displacement is negligible. For this case, the linear tension model can also predict the average normal stress. The power spectral density plot of the nonlinear model at high frequencies reveals many more frequencies, which the linear models cannot predict. Therefore, if we are interested in high frequency phenomenon and/or axial vibration, the nonlinear coupled model is suitable.

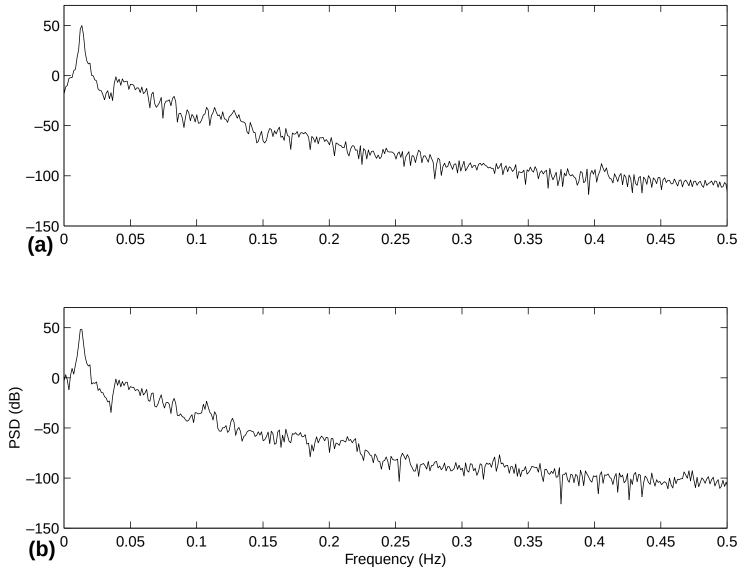

Fig. 22. Forced response: power spectral density plot of $v(L,t)$ when $H_s = 19$ m, $v(X,0) = 0.05X$ and $\dot{v}(X,t) = 0$ for $0 < f < 0.5$ Hz. (a) PSD plot for $v_{\text{linear}}(L,t)$, (b) PSD plot for $v_{\text{nonlinear}}(L,t)$.

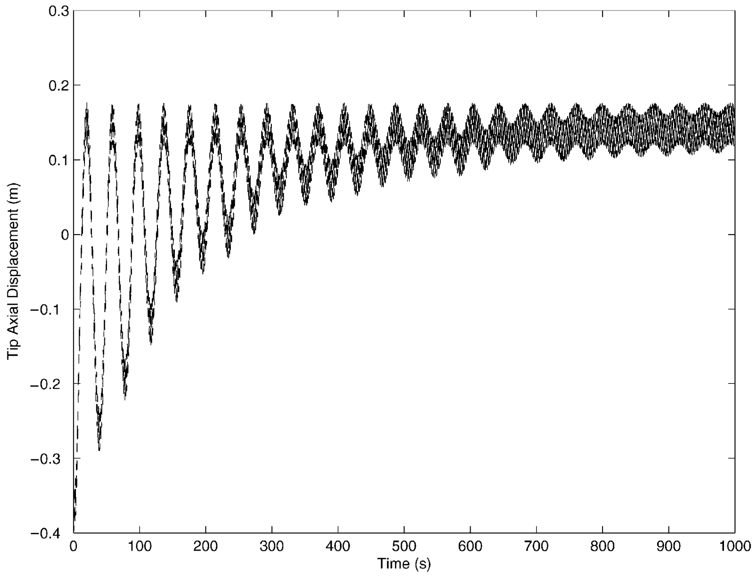

Fig. 23. Forced response: axial displacement $u(L,t)$ when $H_s = 19$ m, $v(X,0) = 0.05X$ and $\dot{v}(X,t) = 0$.

2. When the random transverse force is applied with zero initial conditions, it is observed that the transverse displacements predicted by both models are similar to each other with similar frequency content at low frequencies. Therefore, the responses look identical in this case including the irregular beating phenomenon.

3. When the same random transverse force is applied with nonzero initial conditions, the beating disappears. Instead the subharmonic resonance of order 1/2 is observed. It is observed that first damped natural frequency predicted by the linear tension model is slightly higher than that predicted by the nonlinear coupled model. This is expected of the linear

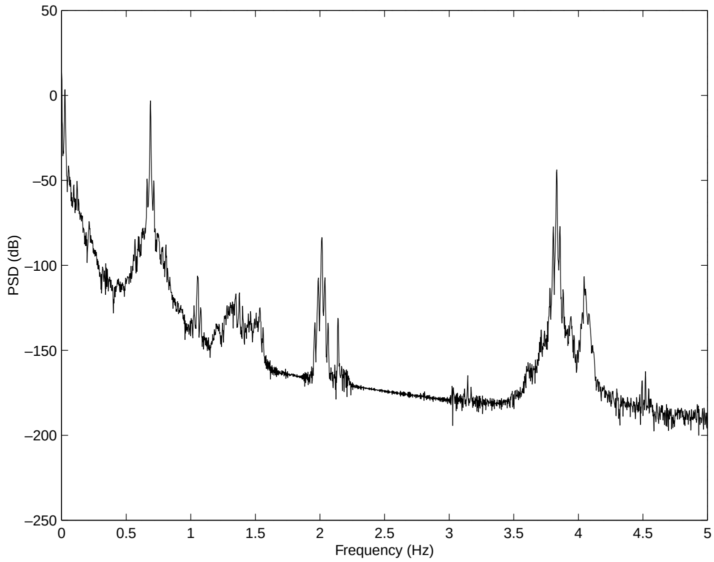

Fig. 24. Forced response: power spectral density plot of $u(L,t)$ when $H_s = 19$ m, $v(X,0) = 0.05X$ and $\dot{v}(X,t) = 0$.

tension model since it is 'stiffer' than the nonlinear coupled model. However, this is the first place we were able to see the difference in the response.

Acknowledgements

This work has been supported by the Office of Naval Research Grant No. N00014-97-1-0017. We thank our project manager Dr. Thomas Swean for his interest and financial supports. The authors are pleased to acknowledge the continued collaboration with their colleague, Professor Timothy Wei.

References

[1] Adrezin R, Bar-Avi P, Benaroya H. Dynamic response of compliant offshore structures – review. J Aerospace Eng 1996;9(4): 114–31.
[2] Jain RK, Kirk CL. Dynamic response of a double articulated offshore loading structure to noncollinear waves and current. J Energy Resour Technol 1981;103:41–7.
[3] Bar-Avi P. Dynamic response of an offshore articulated tower. PhD Thesis, Rutgers, The State University of New Jersey, May 1996.
[4] Bar-Avi P, Benaroya H. Nonlinear dynamics of compliant offshore structures. Lisse, The Netherlands: Swets and Zeitlinger Publishers; 1997.
[5] Adrezin R, Benaroya H. Non-linear stochastic dynamics of tension leg platforms. J Sound Vib 1999;220(1):27–65.
[6] Adrezin R, Benaroya H. Response of a tension leg platform to stochastic wave forces. Probab Eng Mech 1999;14:3–17.
[7] Yigit AS, Christoforou AP. Coupled axial and transverse vibrations of oilwell drillstrings. J Sound Vib 1996;195(4):617–27.
[8] Han SM, Benaroya H. Nonlinear coupled transverse and axial vibration of a compliant structure 1: formulation and free vibration. J Sound Vib 2000;237(5):837–73.
[9] Han SM, Benaroya H. Nonlinear coupled transverse and axial vibration of a compliant structure 2: forced vibration. J Sound Vib 2000;237(5):874–99.
[10] Han SM, Benaroya H. Nonlinear dynamics of an articulated tower. In: 13th ASCE Engineering Mechanics Conference, June 1999.
[11] Meirovitch L. Analytical methods in vibrations. New York: Macmillan; 1967.
[12] Benaroya H. Mechanical vibration. Englewood Cliffs, NJ: Prentice-Hall; 1998.
[13] Morison JR, O'Brien MP, Johnson JW, Schaaf SA. The force exerted by surface waves on piles. Pet Trans, AIME 1950;189: 149–57.

[14] Wilson J. Dynamics of offshore structures. New York: Wiley; 1984.
[15] Chakrabarti S. Hydrodynamics of offshore structures. Computational Mechanics Publications; 1987.
[16] Sverdrup H, Munk W. Wind, sea, and swell: theory of relations for forecasting. US Navy Hydrographic Office, Publication No. 601, 1947.
[17] Borgman LE. Ocean wave simulation for engineering design. J Waterway Harbors Div 1969;95:557–83.
[18] Faulkner D, Chatterjee PC, Das PK. A hydro-structural analysis program for TLPs. Ocean Eng 1977;24(4):313–34.